ACS APPLIED MATERIALS & INTERFACES

Research Article

www.acsami.org

Surface-Mediated Solidification of a Semiconducting Polymer during Time-Controlled Spin-Coating

Jin Yeong Na,[†,‡] Boseok Kang,[†,§] Seung Goo Lee,[⊥] Kilwon Cho,[*,§] and Yeong Don Park[*,‡]

[‡]Department of Energy and Chemical Engineering, Incheon National University, Incheon 22012, Korea

[§]Center for Advanced Soft Electronics and Department of Chemical Engineering, Pohang University of Science and Technology, Pohang 37673, Korea

[⊥]Department of Chemical Engineering, Massachusetts Institute of Technology, Cambridge, Massachusetts 02139, United States

Supporting Information

ABSTRACT: Spin-casting a polymer semiconductor solution over a short period of only a few seconds dramatically improved the molecular ordering and charge transport properties of the resulting semiconductor thin films. In this process, it was quite important to halt spinning before the drying line propagation had begun. Here, we elucidated the effects of the substrate surface characteristics on the drying kinetics during spin-coating, systematically investigated the microstructural evolution during semiconducting polymer solidification, and evaluated the performances of the resulting polymer field-effect transistors. We demonstrated that the spin time required to enhance the molecular ordering and electrical properties of the polythiophene thin films was strongly correlated with the solidification onset time, which was altered by surface treatments introduced onto the substrate surfaces.

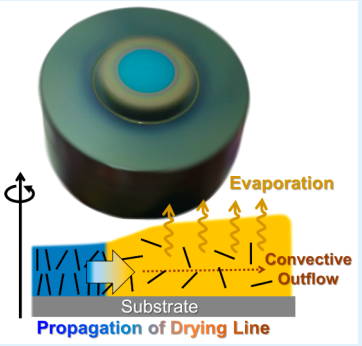

KEYWORDS: *polythiophene, organic field-effect transistor, spin-coating, solidification, surface*

INTRODUCTION

Spin-coating is a technique commonly used to produce thin films of various materials with micrometer to nanometer thicknesses.[1,2] This method is remarkably versatile, inexpensive, easy to use, and highly effective for reproducibly depositing uniform thin films. Because of the advantages of the spin-coating technique, spin-coating is frequently used to deposit an immense variety of solution-processable organic semiconductor materials and to fabricate high-performance organic field-effect transistor (OFET) devices with a high reliability.[3,4] The solid-state order and morphology of a spin-cast organic semiconducting layer has been found to strongly affect the overall OFET performance,[2,5] and a film's properties largely depend on the processing conditions applied during spin-coating, such as the solvent properties,[6,7] the substrate temperature,[8−10] the surface characteristics,[10,11] the ambient solvent vapor pressure,[12] and the spinning speed[13,14] or time.[15] The final film thickness may be predicted to a high accuracy using semiempirical models based on processing parameters (viscosity, concentration, and spin rate),[16,17] whereas nano/mesoscale structures and the physical properties of the resulting film are not readily predictable because of the many mechanisms at work during the spin-coating process.[18,19] A variety of processing conditions can affect the organic semiconductor material solidification process and the associated OFET performances. These processing conditions must be empirically investigated, in a step by step fashion.

In a previous report, we systematically characterized the effects of the spin-coating time (the "spin time") on the microstructural evolution during semiconducting polymer solidification in an effort to establish the relationship between this parameter and the performances of the resulting polymer FETs.[15] A short spin-coating time of a few seconds was shown to dramatically improve the morphology and molecular ordering in a conjugated polymer thin film because the $\pi-\pi$ stacking structures formed by the polymer molecules grew slowly and with a greater degree of order due to the residual solvent present in the slightly wet film. The improved molecular ordering, in turn, improved charge carrier transport in the FETs prepared from these films. Furthermore, the effective spin-time range (i.e., the range of times that provided improved molecular ordering and field-effect mobilities) could be controlled using solvent additives and was related to the physical properties of the additives used. These results prompted us to wonder about the fundamental relationship between the effective spin time and the surface characteristics of the substrates, the latter of which could significantly affect the drying kinetics of a deposited solution and the resulting polymer solidification process. Although many reports have described the effects of a substrate's surface on the resulting OFET performance, to the best of our knowledge, all previous studies were performed using typical spin-coating methods with the course of time. The time-controlled spin-coating method described here provides valuable information

Received: September 17, 2016
Accepted: November 29, 2016
Published: November 29, 2016

DOI: 10.1021/acsami.6b11737
ACS Appl. Mater. Interfaces 2017, 9, 9871−9879

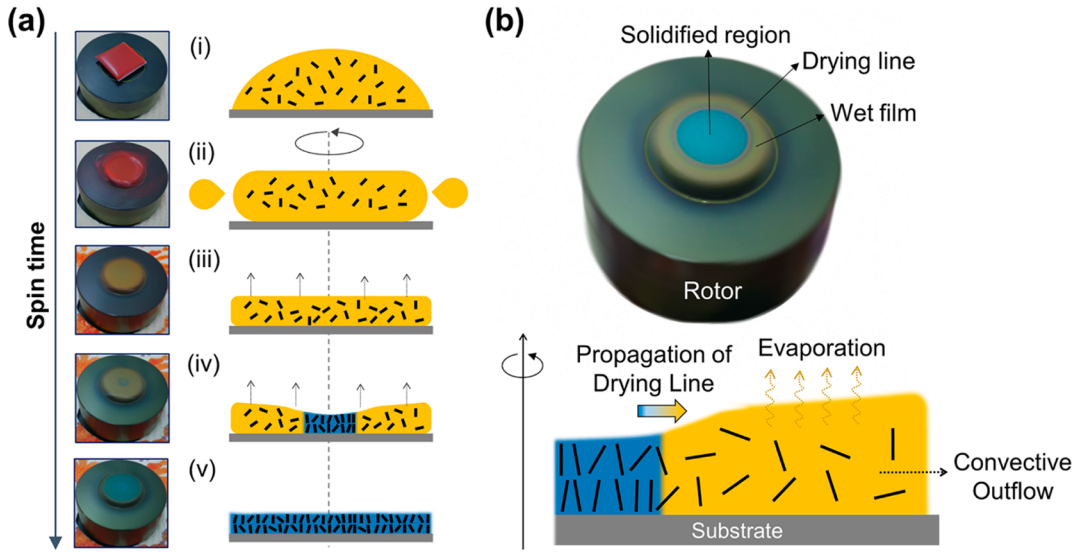

Figure 1. (a) Videomicroscopy images (left) and corresponding schematic illustrations (right) showing the spin-coating steps, in which the solution consisted of P3HT and chlorobenzene solvent. (b) A videomicroscopy image (top) and a schematic diagram (bottom) of an intermediate stage just before film drying had reached completion during spin-coating.

about the kinetics of the spin-coating process, deepens our understanding of the organic semiconductor growth, and establishes rules of thumb for fabricating high-performance OFETs.

In this paper, we systematically studied the relationships between the substrate surface characteristics and the effective spin time during a time-controlled spin-coating step. The substrate surfaces were chemically modified using self-assembled monolayers (SAMs), and the micro and macro structures, morphologies, and optical and electrical characteristics of the spin-cast polymeric semiconductor layers were thoroughly investigated using two-dimensional grazing-incidence X-ray diffraction (2D GIXD), atomic force microscopy (AFM), UV−vis spectroscopy, and transistor device measurements. Notably, hydrophobic substrates and hydrophilic substrates induced dramatically different solidification behaviors in a deposited polymer solution. These behaviors were, in turn, correlated to the microstructure of the polymer thin film and the resulting FET characteristics. Although spin-coating is considered as a technique far from a continuous processing method, the lessons from this study could provide valuable information and keen insight for designing OFET printing processes.

RESULTS AND DISCUSSION

The spin-coating process can be modeled as occurring in four stages:[20] (i) deposition, (ii) spin-up, (iii) spin-off, and (iv) evaporation (Figure 1a). The left column of Figure 1a shows the spin-coating process of a benchmark semiconducting polymer, poly(3-hexylthiophene) (P3HT), from a 1-chlorobenzene (CB) solvent. The deposition process (i) first involved the dispensing of excess amounts of a solution onto a target substrate. In the spin-up stage (ii), the substrate was accelerated to the final spin speed. As the rotational force of the rotor was transferred upward through the fluid, a wavefront formed and flowed to the edge of the substrate under the centrifugal forces, leaving a uniform liquid film behind. After the excess solvent had been flung off the substrate, the fluid was thinned primarily by centrifugal forces until a sufficient amount of solvent had been removed and the viscosity of the liquid layer had increased. This step was called the spin-off stage (iii). In this step, the substrate was spun at a constant rate, and the fluid's viscous forces dominated the fluid thinning behavior. Interference colors were commonly visible at this moment. As the spin-off stage ended, the evaporation stage began (iv). During this step, the centrifugal outflow decreased, and further shrinkage occurred due to solvent loss into the atmosphere. These steps finally resulted in the formation of a thin film on the substrate (v).

A closer examination of the substrate toward the end of the spin-coating process revealed an abrupt color change from the substrate center to the edge (Figure 1b, up). This color change occurred over just a few seconds and was attributed to the propagation of the boundary line of the solidified region (Figure 1b, down). The color of the substrate center was the same as that of the final film, indicating that the region had dried. The differences in the films ahead of and behind the drying line were explored by preparing polymer thin films and intentionally stopping the rotor spinning. Figure 2 plots the normalized UV−vis absorption spectra of the P3HT thin films spin-cast onto hexamethyldisilazane (HMDS)-treated glass substrates over different spinning times (5, 13, or 30 s, respectively). The P3HT thin films spin-cast for 30 s were completely dried during spin-coating, whereas the spinning process of the P3HT thin film cast over 5 s was stopped before the drying line had propagated. The UV−vis spectra of the 5 s-cast P3HT thin film and 30 s-cast film differed significantly. Along with the decreased spinning time from 30 to 5 s, the intensities of the two shoulders at $\lambda = 558$ and 603 nm increased,[21,22] indicating that shorter spinning times led to the development of a larger number of ordered P3HT aggregates that contain interchain $\pi-\pi$ stacking interactions via a tardy growth process in the presence of residual solvent.[15,23] The spectra obtained at the film centers and edges of both thin films were nearly identical, indicating good uniformity among the spin-cast films. The spectra collected at the film center and edge of the 13 s-cast P3HT thin film, which had included both dried and wet regions, revealed huge differences (see the inset of Figure 2). The spectra measured at the film edge revealed developed shoulder peaks similar to those observed in the 5 s-cast films, indicating a larger number of ordered P3HT aggregates.

DOI: 10.1021/acsami.6b11737
ACS Appl. Mater. Interfaces 2017, 9, 9871−9879

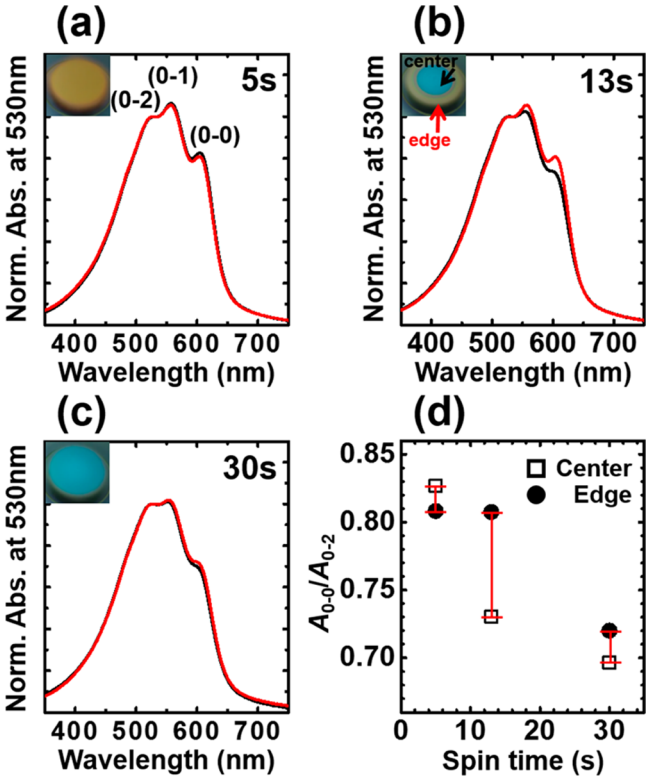

Figure 2. UV−vis absorption spectra showing the normalized absorption bands at the 0−2 transition (λ = 530 nm) in the P3HT thin films spin-cast onto HMDS-treated substrates over various spinning times: (a) 5 s, (b) 13 s, and (c) 30 s. The spectra were measured at the film center (black color) and edge (red color) of the four-square-centimeter samples after the films had completely dried. (d) Intensity ratios between the first (λ = 603 nm) and second (λ = 558 nm) vibronic transitions as a function of the spinning time. The inset shows optical images of the substrates prepared using a solution deposited during spin-coating at specific times.

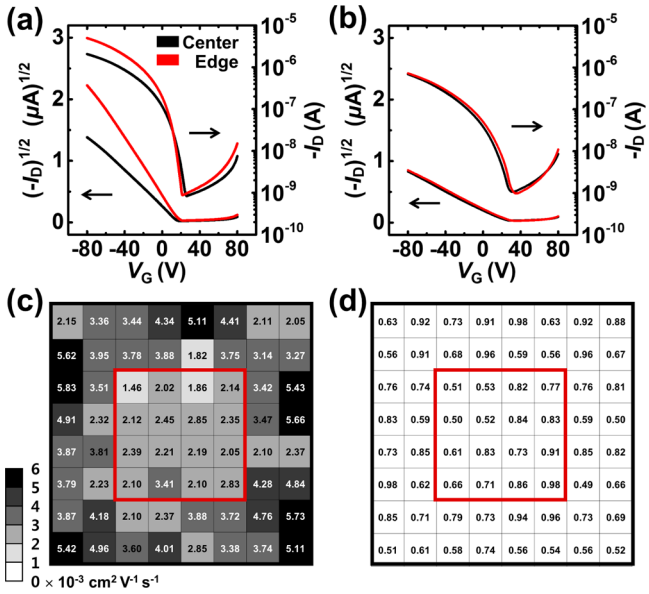

Figure 3. Transfer characteristics (I_D−V_G) and statistical analysis of the evaluated FET mobilities of the OFETs (V_D = −80 V) fabricated using P3HT thin films cast onto HMDS-treated SiO_2/Si substrates, including (a, c) both dried (center) and wet regions (edge), and (b, d) completely dried during spin-coating. The mobility values were measured at sixty-four transistor units on a 1.5 in. square wafer, and the average values were calculated at the film center and edge, as defined by the red-colored box.

The electrical properties collected at the film center and edge were more distinct. We characterized the electrical properties of the OFETs prepared on large-scale HMDS-treated SiO_2/Si substrates (see the Experimental Section for details). Figure 3a and 3b plot the transfer characteristics (the I_D−V_G characteristics) of the OFETs. In the P3HT film that had included both dried and wet regions, the hole mobility at the film edge (average value of $3.8 \pm 0.62 \times 10^{-3}$ cm^2 V^{-1} s^{-1}) was notably higher than the corresponding value at the film center (average value of $2.3 \pm 0.44 \times 10^{-3}$ cm^2 V^{-1} s^{-1}). By contrast, the OFETs prepared from P3HT films that had completely dried during spin-coating exhibited similar mobility values at the film center and edge (average values of $0.73 \pm 0.14 \times 10^{-3}$ and $0.72 \pm 0.14 \times 10^{-3}$ cm^2 V^{-1} s^{-1}, respectively). The statistical profile of the FET mobilities measured across sixty-four transistor units on a large scaled wafer (1.5 in. square) revealed a dramatic spread (Figure 3c, d). These results indicated that a brief spin time of a few seconds was fairly effective at improving the field-effect mobility.

We next examined the effects of the substrate surfaces on the film drying behaviors. To this end, substrate surfaces were modified using HMDS or hydrophobic octadecyltrichlorosilane (ODTS) (Figure 4a−c), respectively. The hydrophilic clean SiO_2/Si substrates (denoted OH) were prepared simultaneously for comparison. We then monitored the spin-coating process of the P3HT/CB solution on the three substrates using optical videomicroscopy. The initiation (t_{onset}) and completion (t_{end}) times associated with the solidification process, which proceeded from the film center to the edge, were carefully determined from an analysis of the recorded video files, and the results are summarized as a function of the surface energies in Figure 4d. The surface energies of the substrates were evaluated from the measured water contact angles, and were found to be 60.0, 43.6, or 28.1 mJ/m^2 for bare SiO_2, HMDS-treated, or ODTS-treated substrates, respectively.[24] We found that t_{onset} increased although the total solidification time (defined as $t_{onset} - t_{end}$) decreased as the surface energy of the substrate increased. In other words, substrates with a low surface energy delayed the initiation of solidification and reduced the solidifying time. The propagation velocities, defined as the path length of the drying line per unit solidification time, were found to be 0.270 (for OH), 0.377 (for HMDS), and 0.382 cm s^{-1} (for ODTS), respectively.

The early initiation of solidification on the high surface energy substrate could be understood as arising from heterogeneous nucleation.[25,26] Heterogeneous nucleation occurs much more often than homogeneous nucleation. High-energy surfaces can promote nucleation because of their wetting properties; contact angles greater than zero between phases facilitate particle nucleation. The free energy needed for heterogeneous nucleation is equal to the product of the homogeneous nucleation and a function of the contact angle (θ)[27]

$$\Delta G_{heterogeneous} = \Delta G_{homogeneous} \cdot f(\theta) \quad (1)$$

where $f(\theta) = (2 - 3\cos\theta + \cos^3\theta)/4$. The barrier energy needed for nucleation can be reduced efficiently. The wetting angle determines the ease of nucleation by reducing the energy needed. The characteristics of the bare SiO_2 surface were quite different from those of the hydrocarbon-modified surfaces of the HMDS- or ODTS-treated substrates and tended to decrease the chemical homogeneity of the polymer solution near the substrate surface. P3HT solidification, therefore, was facilitated in a manner similar

DOI: 10.1021/acsami.6b11737
ACS Appl. Mater. Interfaces 2017, 9, 9871−9879

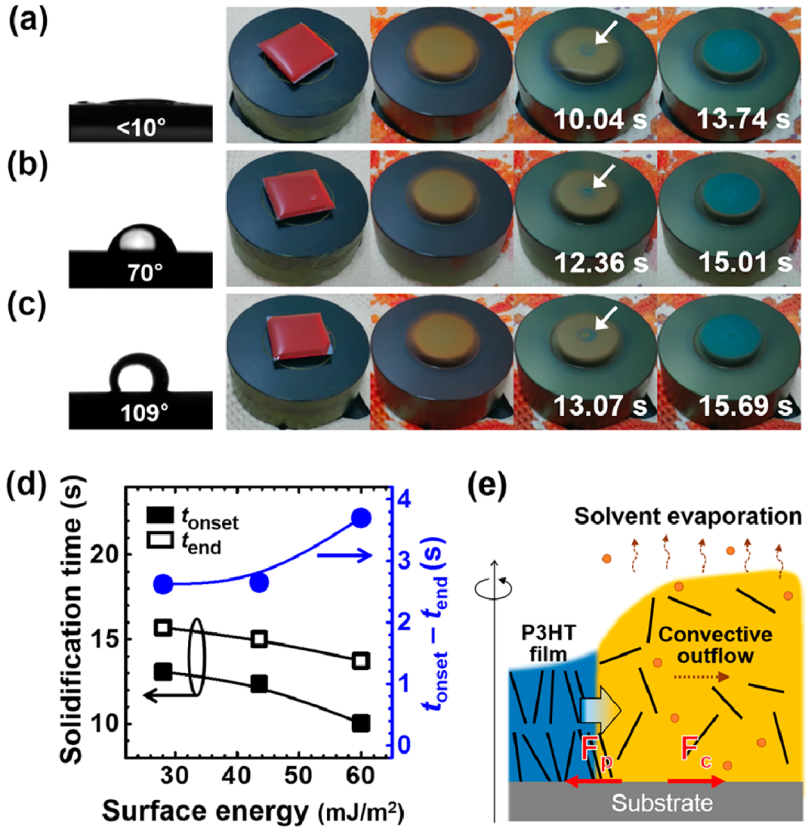

Figure 4. Optical images of the water contact angle measurements on (a) clean SiO_2/Si substrates, (b) HMDS-treated substrates, and (c) ODTS-treated substrates, and a series of videomicroscopy images of the spin-coating process on the corresponding substrates at specific times after initiation. The arrows designate the initiation of P3HT solidification. (d) Summary of the optical monitoring analysis on the three different substrates as a function of the surface energies. (e) Schematic illustration of an intermediate stage just before film drying had reached completion during spin-coating. The drying line propagated along the radial direction. In the drawing, $\mathbf{F}_p$ and $\mathbf{F}_c$ denote the pinning force and centrifugal force, and the red arrows represent only the force directions.

to the earlier nucleation of P3HT in the P3HT and phenyl-C_{61}-butyric acid methyl ester blend, in contrast with the homo P3HT solution.[28,29]

Longer total solidification times or reduced propagation velocities were attributed to the application of a pinning force ($\mathbf{F}_p$) to the liquid layer.[30] As discussed above, the thickness of the coated liquid film decreased due to solvent evaporation and fluid flow along the radial direction. The evaporation of solvent molecules was expected to be uniform across the substrates and nearly identical, regardless of the substrate surface. A weak centrifugal force ($\mathbf{F}_c$) at this time scale gave rise to a convective outflow and assisted in the propagation of the observed drying line, whereas $\mathbf{F}_p$ impeded the convective outflow. Because adhesion of a liquid layer (mainly CB) to a high-energy surface is strong, a larger $\mathbf{F}_p$ on such a surface would effectively suppress the propagation of the drying boundary line. We concluded that the substrates with high surface energies accelerated solidification initiation and extended the solidifying time during spin-coating.

The solvent drying behavior during spin-casting was crucial for the thin-film formation and the development of favorable film morphologies and crystalline domains.[23,31] The effects of brief spinning times on three different substrates were investigated by measuring the UV−vis absorption spectra of P3HT thin films (Figure 5a−c). As in the UV−vis spectra presented in Figure 2, these spectra displayed a dominant peak at λ = 530 nm with two minor shoulders at lower energies (λ = 558 and 603 nm).[21,32] As the spin time was decreased from 30 to 5 s, the intensities of the two shoulder peaks gradually increased, regardless of the substrate. Importantly, on the low energy surface, the observed intensity ratio between the first and second vibronic transitions tended to be slightly higher than that on the substrate with a high surface energy (Figure 5d). These features were related to an increase in the number of ordered aggregates associated with interchain $\pi-\pi$ stacking of P3HT.[33] The effects of short solidification times on the ODTS-treated substrate indicated that the development of ordered P3HT aggregates was comparable to or superior to aggregate development on a bare SiO_2 substrate. Furthermore, we found that the threshold spin time required to enhance the molecular ordering of P3HT agreed well with the t_{onset} values observed in the videomicroscopy results (the inset of Figure 5d). These results demonstrated that the effective range of the spin time could be altered along with the substrate characteristics.

The crystalline structures of the P3HT films were further investigated in detail by using two-dimensional grazing incidence X-ray diffraction (2D GIXD) measurements. Figure 6a presents the 2D GIXD patterns measured from the P3HT thin films spin-coated onto different substrates over different spinning times. All P3HT films showed strong X-ray diffraction peaks along the q_z and q_{xy} axes, respectively, which corresponded to an intermolecular backbone layer ($(h00)$ planes) of 16.1−17.2 Å and a $\pi-\pi$ stacking plane ((010) plane) distance of 3.8 Å.[34,35] The crystallographic information is provided in detail in Table S1. These results revealed that a majority of the P3HT molecules

DOI: 10.1021/acsami.6b11737
ACS Appl. Mater. Interfaces 2017, 9, 9871−9879

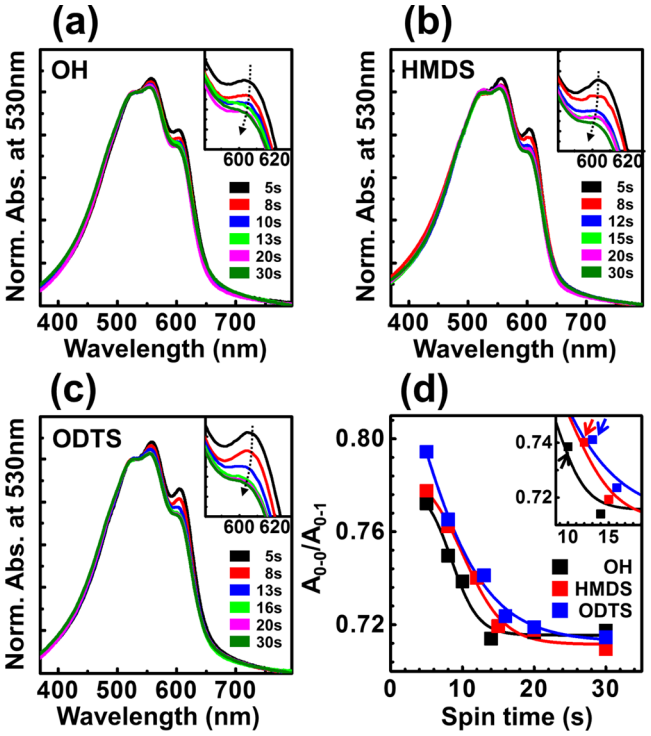

Figure 5. UV−vis absorption spectra showing the normalized absorption bands at the 0−2 transition (λ = 530 nm) in the P3HT thin films spin-cast onto (a) bare SiO_2 substrates, (b) HMDS-treated substrates, and (c) ODTS-treated substrates for various spinning times. The inset shows the magnified view near the first transition at λ = 603 nm. (d) Intensity ratios between the first (λ = 603 nm) and second (λ = 558 nm) vibronic transitions as a function of the spinning time. The inset highlights the difference between the onset points marking the beginning of the intensity ratio reduction. The spin-coating time increased along the direction indicated by the arrow.

adopted an edge-on backbone orientation with side chains normal to the dielectric substrate.[36,37] The degrees of relative crystallinity in these films depended on the spin time, regardless of the substrate, as shown in the 1D X-ray intensity profiles extracted from the 2D GIXD patterns (Figures 6b−6e). The intensity trend for out-of-plane (100) peaks was similar to that of in-plane (010) peaks. Given that the film thickness values were similar (~37 nm), irreverent to the spinning time and substrate (see Figure S1), the intensities of the X-ray reflections were closely related with the degree of relative crystallinity in the films.[31] The intensity increases indicated that the P3HT thin films were more crystalline if prepared using shorter spin times. These results are in good agreement with the UV−vis spectra (Figure 5) and morphological changes observed (see the atomic force microscopy (AFM) images Figure S2). The root-mean-square (RMS) roughness values of the thin films were inclined to increase at shorter spinning times. Interestingly, the molecular order along both the lamellar and $\pi-\pi$ stacking directions were significantly higher on the ODTS-treated substrates. Because the estimated P3HT crystallite sizes were similar across all three substrates (Table S1), the increased relative crystallinity was mainly attributed to a larger number of ordered P3HT aggregates, consistent with the UV−vis spectral results. The enhanced ordering of the P3HT on the ODTS-treated substrates was consistent with the simulation results reported by Gee and co-workers.[38] Video microscopy, UV−vis spectroscopy, and 2D GIXD results together indicated that the relative crystallinities of the P3HT thin films were better on substrate with a low surface energy, despite the shorter total solidification time.

Finally, the charge-transport characteristics of the P3HT thin films were measured by using the transfer curves of OFETs prepared on an 0.8 in. square wafer (Figure 7a−c). Among the series of OFETs, devices prepared with P3HT and spin-coated for 5 s showed the highest average mobility values of 0.0046 (for bare SiO_2), 0.022 (for HMDS-treated SiO_2), and 0.094 (for

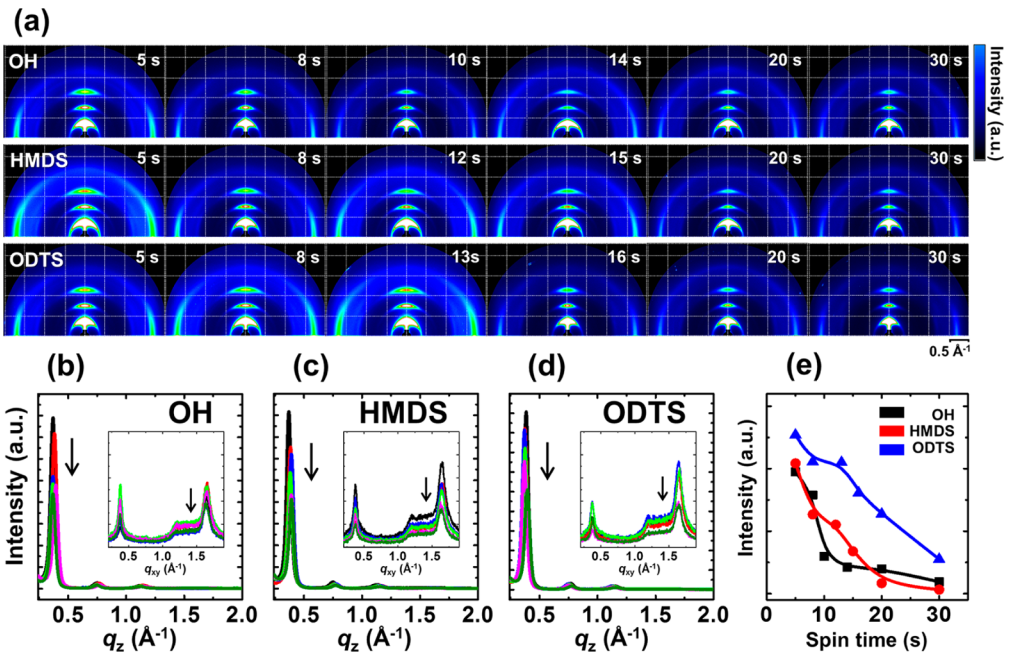

Figure 6. (a) 2D GIXD patterns obtained from the P3HT thin films that had been spin-cast for various spinning times onto the three different substrates. The spinning time increased from 5 to 30 s, moving from the left toward the right figure. (b−d) Extracted X-ray intensity 1D profiles along the out-of-plane and in-plane directions (insets). (e) Areal intensities of the (100) peaks as a function of the spinning time. Spin-coating time increases along the direction indicated by the arrow.

DOI: 10.1021/acsami.6b11737
ACS Appl. Mater. Interfaces 2017, 9, 9871−9879

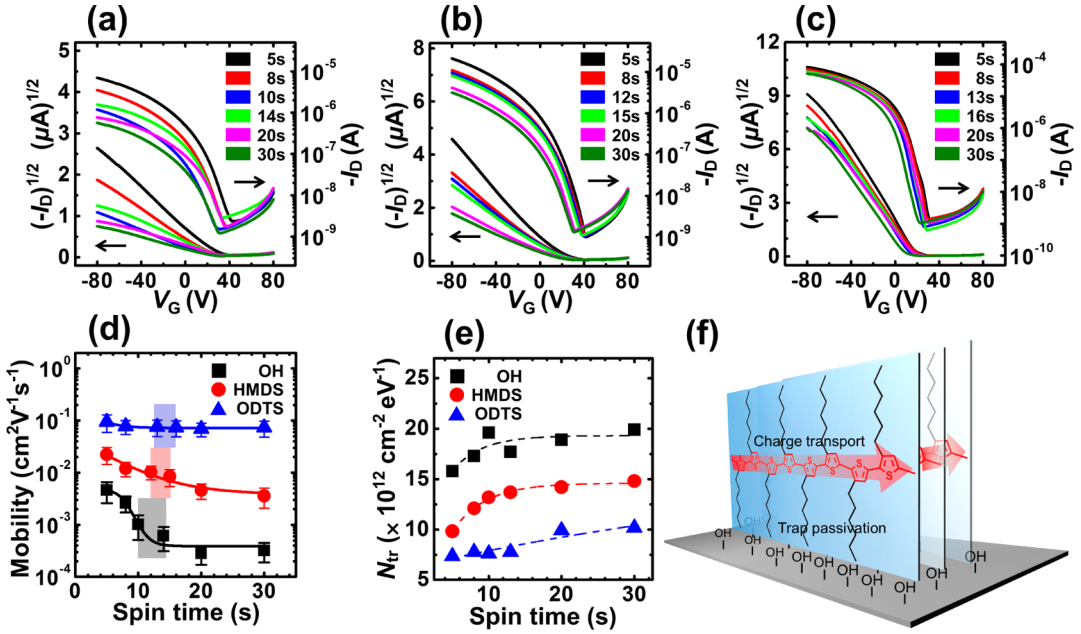

Figure 7. Transfer characteristics (I_D−V_G) of OFETs (V_D = −80 V) fabricated using P3HT thin films that had been spin-cast for various spinning times. The P3HT thin films were spin-coated onto (a) bare SiO_2 substrates (OH), (b) HMDS-treated substrates, and (c) ODTS-treated substrates, respectively. (d) Field-effect mobilities and (e) maximum interface trap densities (N_{tr}) estimated from the I_D−V_G curves as a function of the spinning time. (f) Schematic diagram showing a P3HT crystal with ordered hexyl side chains passivating the charge traps on bare SiO_2/Si substrates.

Table 1. Performances of OFETs Prepared Using the P3HT Thin Films Spin-Cast onto Different Substrates over Various Spin Times[a]

condition						
substrate	spin time (s)	μ_{avg}[b] (cm^2/V s)	V_T[c] (V)	I_{on}/I_{off}[d]	S[e] (V/dec)	N_{tr}[f] (× 10^{12} cm^{-2} eV^{-1})
OH	5	4.6 × 10^{-3}	26.0	3.0 × 10^3	14.1	15.8
	8	2.6 × 10^{-3}	24.2	2.0 × 10^3	15.4	17.3
	10	1.0 × 10^{-3}	21.9	7.8 × 10^2	17.4	19.6
	14	6.1 × 10^{-4}	30.7	5.5 × 10^2	15.7	17.7
	20	2.8 × 10^{-4}	32.6	4.4 × 10^2	16.7	18.9
	30	3.2 × 10^{-4}	28.6	4.7 × 10^2	17.6	19.9
HMDS	5	2.2 × 10^{-2}	12.9	2.1 × 10^4	8.7	9.8
	8	1.2 × 10^{-2}	11.6	9.8 × 10^3	10.8	12.1
	12	1.0 × 10^{-2}	11.6	9.1 × 10^3	11.7	13.2
	15	8.4 × 10^{-3}	13.1	7.3 × 10^3	12.1	13.7
	20	4.6 × 10^{-3}	10.5	2.8 × 10^3	12.6	14.2
	30	3.6 × 10^{-3}	10.7	2.4 × 10^3	13.2	14.8
ODTS	5	9.4 × 10^{-2}	18.0	6.3 × 10^4	6.6	7.4
	8	7.8 × 10^{-2}	19.2	5.0 × 10^4	6.9	7.8
	13	7.6 × 10^{-2}	15.2	7.7 × 10^4	6.8	7.6
	16	7.4 × 10^{-2}	18.0	6.7 × 10^4	6.9	7.8
	20	6.9 × 10^{-2}	16.8	4.9 × 10^4	8.8	9.9
	30	7.4 × 10^{-2}	10.3	4.9 × 10^4	9.1	10.0

[a]Here, OH denotes the bare SiO_2/Si substrates. [b]Average hole mobility in the saturation regime (V_D = −80 V). [c]Threshold voltage. [d]On−off current ratio. [e]Subthreshold slope. [f]Maximum interfacial trap density estimated from the subthreshold slope.

ODTS-treated SiO_2) cm^2 V^{-1} s^{-1} on each substrate, respectively. With longer spinning times, the mobility values steadily decreased and reached a saturating value (Figure 7d and Table 1), which agrees well with the UV−vis spectra and 2D GIXD results.[39] The thresholds of the effective spin times, that is, the effective spin times that provided good FET mobilities, substantially followed the observed t_{onset} values. These results demonstrated that intentionally halting the spin-casting process before the drying line had propagated was quite important for improving the performances of OFETs prepared with semi-crystalline polymer semiconductors. It is noteworthy that the high mobility values of all 5 s-cast P3HT thin films were obtained without the use of any post-treatments, such as thermal annealing or solvent vapor annealing.

The improved mobilities, obtained with the use of short spinning times, were more pronounced on the bare SiO_2 substrate than on the others, most likely due to trap passivation effects among the highly ordered alkyl side chains. The standard dry thermally grown SiO_2 layer included ~5 × 10^{13} cm^{-2} silanol (SiOH) groups on its surface.[40] The SiOH groups have been

DOI: 10.1021/acsami.6b11737
ACS Appl. Mater. Interfaces 2017, 9, 9871−9879

shown to act as electrochemical traps for the injected electrons that form immobile surface Si−O$^-$ ions. These traps may be passivated to some extent by adopting alkyl SAMs on the SiO_2 surfaces.[41,42] Likewise, ordered hexyl side chains of the edge-on P3HT crystallites were thought to partly eliminate charge trapping of the surface SiOH groups. To support our claim, we calculated the maximum interfacial trap density from the subthreshold slope of the devices using the following equation[43−45]

$$N_{tr} = \frac{C_i}{q}\left[\frac{qS}{k_B T \ln(10)} - 1\right] \quad (2)$$

where q is the elementary charge, S is the subthreshold slope (V decade^{-1}), k_B is Boltzmann's constant, and C_i is the capacitance of the gate dielectric (10.8 nF cm^{-2}). The calculated N_{tr} decreased from 19.9 × 10^{12} (for a spinning time of 30 s) to 15.8 × 10^{12} cm^{-2} eV^{-1} (for a spinning time of 5 s) on the bare SiO_2 substrates (Figure 7e). The number of traps present on the bare SiO_2 substrate was about 1 order of magnitude higher than the corresponding values on the other substrates. Given that the relative crystallinities obtained on the bare and HMDS substrates were improved to similar degrees, this huge reduction in the number of traps was attributed to the presence of fewer trapping sites at the semiconductor−dielectric interface as a result of improved self-organization in P3HT films prepared for short spinning times, as discussed above (Figure 7f).[46,47]

CONCLUSIONS

In conclusion, the OFET performances prepared using crystalline polymer semiconductors may be efficiently improved by spin-coating the semiconductor solution for a short period of only a few seconds. In this process, halting the spinning before the drying line had propagated was quite important. We found that the effective spin times needed to obtain enhanced molecular ordering and FET mobilities in P3HT thin films was strongly correlated with the solidification onset time, which depended on the surface characteristics of the substrates. On all substrates, $\pi-\pi$ stacking and lamellar stacking interactions in the P3HT films were significantly enhanced by the tardy growth process resulting from the presence of residual solvent after a short spin-coating time. Nonetheless, the improvements observed in the device performances were most pronounced in films prepared on the hydrophilic bare SiO_2/Si substrates, due to the trap passivation effects of the well-ordered hexyl side chains of the P3HT crystallites. These results deepen our knowledge of polymer semiconductors, and our simple method for improving molecular ordering is definitely useful for the development of robust and high-performance plastic semiconductor devices.

EXPERIMENTAL SECTION

Preparation of P3HT Thin Films and Transistor Devices. Poly(3-hexylthiophene) (P3HT, regioregularity of ∼95%, molecular weight M_w of 37 kDa) and 1-chlorobenzene (CB) were purchased from Rieke Metals, Inc. and Sigma-Aldrich, Inc., respectively and were used as received without further purification. Highly doped Si was used as a substrate and as a gate electrode. A 300 nm-thick SiO_2 layer was used as a gate dielectric. The SiO_2/Si substrates were modified to tune their surface energies via piranha solution cleaning and hexamethyldisilazane (HMDS, Sigma−Aldrich, Inc.) and octadecyltrichlorosilane (ODTS, Gelest) treatments, respectively.[10] A P3HT solution (14 mg mL^{-1} in CB) was prepared in sealed vials to avoid the solvent evaporation during dissolution at 40 °C. The warm P3HT solution was allowed to reach room temperature prior to use. P3HT thin films were spin-coated at 1200 rpm over various spin times (5−30 s) (Spin-1200D, Midas) and were dried in vacuum. P3HT FETs were formed by evaporating gold source/drain electrodes through a metal mask (channel width = 2000 μm and channel length =100 μm). For the UV−vis absorption measurements, identical P3HT films were prepared on transparent glass substrates in place of SiO_2/Si wafers with the same surface treatments.

Thin-Film Characterization. The thickness values of the cast P3HT films were measured using an ellipsometer (J. A. Woollam Co. Inc.). UV−vis absorption spectra were obtained by using a UV−vis spectrophotometer (CARY-5000, Varian). Water contact angle measurements were collected on the modified substrates using a drop shape analysis system (Krüss).[24] The surface energies of the SiO_2 substrates were analyzed by measuring the contact angle using deionized water, glycerol, and diiodomethane after various surface treatments. The surface energies were calculated from the three liquids, each with different polarities. Morphologies of the films were characterized by atomic force microscopy (AFM, Multimode 8, Digital Instruments). Two-dimensional grazing incidence X-ray diffraction (2D GIXD) patterns were measured at the 3C and 9A beamlines of the Pohang Accelerator Laboratory (PAL), Korea. The 2D GIXD sample stage is equipped with a 7-axis motorized stage for the fine alignment of samples and the incidence angle of X-ray beam (wavelength of 1.103 Å) was set to 0.11° close to the critical angle of P3HT. 2D GIXD patterns were recorded using a 2D CCD detector over X-ray irradiation time of 10−30 s dependent on the saturation level of the detector. Diffraction angles were calibrated by a precalibrated reference, sucrose. The OFET performances were characterized using a semiconductor analyzer (Keithley 4200) at room temperature. The field-effect mobility (μ) and threshold voltage (V_T) values were estimated in the saturation regime (V_D = −80 V) according to the equation[48]

$$I_D = \frac{W}{2L}\mu C_i (V_G - V_T)^2 \quad (3)$$

where I_D is the drain current, V_G is the gate−source voltage, and C_i is the capacitance of the gate dielectric (10.8 nF cm^{-2}).

ASSOCIATED CONTENT

Supporting Information

The Supporting Information is available free of charge on the ACS Publications website at DOI: 10.1021/acsami.6b11737.

Film thickness values, AFM images, and detailed crystallographic information for the P3HT thin films (PDF)

AUTHOR INFORMATION

Corresponding Authors

*E-mail: ydpark@inu.ac.kr.

*E-mail: kwcho@postech.ac.kr.

ORCID

Kilwon Cho: 0000-0003-0321-3629

Yeong Don Park: 0000-0002-1615-689X

Author Contributions

†J.Y.N. and B.K. contributed equally to this work.

Notes

The authors declare no competing financial interest.

ACKNOWLEDGMENTS

This research was supported by the Incheon National University Research Grant in 2014 and a grant (Code 2011−0031628) from the Center for Advanced Soft Electronics under the Global Frontier Research Program of the Ministry of Science, ICT and Future Planning, Korea. The authors thank the Pohang Accelerator Laboratory for providing the synchrotron radiation sources at 3C, 5A, 9A, and 9C beamlines used in this study.

DOI: 10.1021/acsami.6b11737
ACS Appl. Mater. Interfaces 2017, 9, 9871−9879

REFERENCES

(1) Kang, B.; Lee, W. H.; Cho, K. Recent Advances in Organic Transistor Printing Processes. *ACS Appl. Mater. Interfaces* **2013**, *5*, 2302−2315.

(2) Dong, H. L.; Fu, X. L.; Liu, J.; Wang, Z. R.; Hu, W. 25th Anniversary Article: Key Points for High-Mobility Organic Field-Effect Transistors. *Adv. Mater.* **2013**, *25*, 6158−6182.

(3) Cho, J. H.; Lee, J.; Xia, Y.; Kim, B.; He, Y. Y.; Renn, M. J.; Lodge, T. P.; Frisbie, C. D. Printable Ion-Gel Gate Dielectrics for Low-Voltage Polymer Thin-Film Transistors on Plastic. *Nat. Mater.* **2008**, *7*, 900−906.

(4) Yan, H.; Chen, Z. H.; Zheng, Y.; Newman, C.; Quinn, J. R.; Dotz, F.; Kastler, M.; Facchetti, A. A High-Mobility Electron-Transporting Polymer for Printed Transistors. *Nature* **2009**, *457*, 679−U671.

(5) Tsao, H. N.; Cho, D.; Andreasen, J. W.; Rouhanipour, A.; Breiby, D. W.; Pisula, W.; Mullen, K. The Influence of Morphology on High-Performance Polymer Field-Effect Transistors. *Adv. Mater.* **2009**, *21*, 209−212.

(6) Chang, J. F.; Sun, B. Q.; Breiby, D. W.; Nielsen, M. M.; Solling, T. I.; Giles, M.; McCulloch, I.; Sirringhaus, H. Enhanced Mobility of Poly(3-Hexylthiophene) Transistors by Spin-Coating from High-Boiling-Point Solvents. *Chem. Mater.* **2004**, *16*, 4772−4776.

(7) Park, Y. D.; Lee, H. S.; Choi, Y. J.; Kwak, D.; Cho, J. H.; Lee, S.; Cho, K. Solubility-Induced Ordered Polythiophene Precursors for High-Performance Organic Thin-Film Transistors. *Adv. Funct. Mater.* **2009**, *19*, 1200−1206.

(8) Chabinyc, M. L.; Wong, W. S.; Arias, A. C.; Ready, S.; Lujan, R. A.; Daniel, J. H.; Krusor, B.; Apte, R. B.; Salleo, A.; Street, R. A. Printing Methods and Materials for Large-Area Electronic Devices. *Proc. IEEE* **2005**, *93*, 1491−1499.

(9) Moonen, P. F.; Yakimets, I.; Huskens, J. Fabrication of Transistors on Flexible Substrates: From Mass-Printing to High-Resolution Alternative Lithography Strategies. *Adv. Mater.* **2012**, *24*, 5526−5541.

(10) Lim, J. A.; Lee, W. H.; Kwak, D.; Cho, K. Evaporation-Induced Self-Organization of Inkjet-Printed Organic Semiconductors on Surface-Modified Dielectrics for High-Performance Organic Transistors. *Langmuir* **2009**, *25*, 5404−5410.

(11) Kim, D. H.; Park, Y. D.; Jang, Y. S.; Yang, H. C.; Kim, Y. H.; Han, J. I.; Moon, D. G.; Park, S. J.; Chang, T. Y.; Chang, C. W.; Joo, M. K.; Ryu, C. Y.; Cho, K. Enhancement of Field-Effect Mobility Due to Surface-Mediated Molecular Ordering in Regioregular Polythiophene Thin Film Transistors. *Adv. Funct. Mater.* **2005**, *15*, 77−82.

(12) Kim, D. H.; Park, Y. D.; Jang, Y.; Kim, S.; Cho, K. Solvent Vapor-Induced Nanowire Formation in Poly(3-Hexylthiophene) Thin Films. *Macromol. Rapid Commun.* **2005**, *26*, 834−839.

(13) Choi, D.; Ahn, B.; Kim, S. H.; Hong, K.; Ree, M.; Park, C. E. High-Performance Triisopropylsilylethynyl Pentacene Transistors Via Spin Coating with a Crystallization-Assisting Layer. *ACS Appl. Mater. Interfaces* **2012**, *4*, 117−122.

(14) Kotsuki, K.; Tanaka, H.; Obata, S.; Stauss, S.; Terashima, K.; Saiki, K. The Importance of Spinning Speed in Fabrication of Spin-Coated Organic Thin Film Transistors: Film Morphology and Field Effect Mobility. *Appl. Phys. Lett.* **2014**, *104*, 233306−233309.

(15) Na, J. Y.; Kang, B.; Sin, D. H.; Cho, K.; Park, Y. D. Understanding Solidification of Polythiophene Thin Films During Spin-Coating: Effects of Spin-Coating Time and Processing Additives. *Sci. Rep.* **2015**, *5*, 13288−13301.

(16) Bornside, D. E.; Macosko, C. W.; Scriven, L. E. Spin Coating: One-Dimensional Model. *J. Appl. Phys.* **1989**, *66*, 5185−5193.

(17) Flack, W. W.; Soong, D. S.; Bell, A. T.; Hess, D. W. A Mathematical Model for Spin Coating of Polymer Resists. *J. Appl. Phys.* **1984**, *56*, 1199−1206.

(18) Norrman, K.; Ghanbari-Siahkali, A.; Larsen, N. B. 6 Studies of Spin-Coated Polymer Films. *Annu. Rep. Prog. Chem., Sect. C: Phys. Chem.* **2005**, *101*, 174−201.

(19) Park, Y. D.; Park, J. K.; Lee, W. H.; Kang, B.; Cho, K.; Bazan, G. C. Post-Deposition Dipping Method for Improving the Electronic Properties of a Narrow Bandgap Conjugated Polymer. *J. Mater. Chem.* **2012**, *22*, 11462−11465.

(20) Sahu, N.; Parija, B.; Panigrahi, S. Fundamental Understanding and Modeling of Spin Coating Process: A Review. *Indian. J. Phys.* **2009**, *83*, 493−502.

(21) Oosterbaan, W. D.; Vrindts, V.; Berson, S.; Guillerez, S.; Douheret, O.; Ruttens, B.; D'Haen, J.; Adriaensens, P.; Manca, J.; Lutsen, L.; Vanderzande, D. Efficient Formation, Isolation and Characterization of Poly(3-Alkylthiophene) Nanofibres: Probing Order as a Function of Side-Chain Length. *J. Mater. Chem.* **2009**, *19*, 5424−5435.

(22) Malik, S.; Nandi, A. K. Thermodynamic and Structural Investigation of Thermoreversible Poly(3-Dodecyl Thiophene) Gels in the Three Isomers of Xylene. *J. Phys. Chem. B* **2004**, *108*, 597−604.

(23) Yang, H. C.; Shin, T. J.; Yang, L.; Cho, K.; Ryu, C. Y.; Bao, Z. N. Effect of Mesoscale Crystalline Structure on the Field-Effect Mobility of Regioregular Poly(3-Hexyl Thiophene) in Thin-Film Transistors. *Adv. Funct. Mater.* **2005**, *15*, 671−676.

(24) Lim, S. C.; Kim, S. H.; Lee, J. H.; Kim, M. K.; Kim, D. J.; Zyung, T. Surface-Treatment Effects on Organic Thin-Film Transistors. *Synth. Met.* **2005**, *148*, 75−79.

(25) Siegel, J.; Solis, J.; Afonso, C. N.; Vega, F.; Bankmann, J.; Sacristan, O. M.; Sokolowski-Tinten, K. Evidence for Surface Initiated Solidification in Ge Films Upon Picosecond Laser Pulse Irradiation. *J. Appl. Phys.* **2001**, *89*, 3642−3649.

(26) Joshi, Y. M.; Shahin, A.; Cates, M. E. Delayed Solidification of Soft Glasses: New Experiments, and a Theoretical Challenge. *Faraday Discuss.* **2012**, *158*, 313−324.

(27) Mittal, K. L. *Advances in Contact Angle, Wettability and Adhesion*; Wiley: New York, 1983; Vol. *1*.

(28) Chou, K. W.; Yan, B. Y.; Li, R. P.; Li, E. Q.; Zhao, K.; Anjum, D. H.; Alvarez, S.; Gassaway, R.; Biocca, A.; Thoroddsen, S. T.; Hexemer, A.; Amassian, A. Spin-Cast Bulk Heterojunction Solar Cells: A Dynamical Investigation. *Adv. Mater.* **2013**, *25*, 1923−1929.

(29) Shin, N.; Richter, L. J.; Herzing, A. A.; Kline, R. J.; DeLongchamp, D. M. Effect of Processing Additives on the Solidification of Blade-Coated Polymer/Fullerene Blend Films Via in-Situ Structure Measurements. *Adv. Energy Mater.* **2013**, *3*, 938−948.

(30) Wu, J.; Xia, J.; Lei, W.; Wang, B. P. Advanced Understanding of Stickiness on Superhydrophobic Surfaces. *Sci. Rep.* **2013**, *3*, 3268−3271.

(31) Kim, G.; Kang, S. J.; Dutta, G. K.; Han, Y. K.; Shin, T. J.; Noh, Y. Y.; Yang, C. A Thienoisoindigo-Naphthalene Polymer with Ultrahigh Mobility of 14.4 Cm(2)/V.S That Substantially Exceeds Benchmark Values for Amorphous Silicon Semiconductors. *J. Am. Chem. Soc.* **2014**, *136*, 9477−9483.

(32) Li, G.; Yao, Y.; Yang, H.; Shrotriya, V.; Yang, G.; Yang, Y. "Solvent Annealing" Effect in Polymer Solar Cells Based on Poly(3-Hexylthiophene) and Methanofullerenes. *Adv. Funct. Mater.* **2007**, *17*, 1636−1644.

(33) Masri, Z.; Ruseckas, A.; Emelianova, E. V.; Wang, L. J.; Bansal, A. K.; Matheson, A.; Lemke, H. T.; Nielsen, M. M.; Nguyen, H.; Coulembier, O.; Dubois, P.; Beljonne, D.; Samuel, I. D. W. Molecular Weight Dependence of Exciton Diffusion in Poly(3-Hexylthiophene). *Adv. Energy Mater.* **2013**, *3*, 1445−1453.

(34) Kline, R. J.; Mcgehee, M. D.; Toney, M. F. Highly Oriented Crystals at the Buried Interface in Polythiophene Thin-Film Transistors. *Nat. Mater.* **2006**, *5*, 222−228.

(35) Jimison, L. H.; Himmelberger, S.; Duong, D. T.; Rivnay, J.; Toney, M. F.; Salleo, A. Vertical Confinement and Interface Effects on the Microstructure and Charge Transport of P3ht Thin Films. *J. Polym. Sci., Part B: Polym. Phys.* **2013**, *51*, 611−620.

(36) Kim, H. G.; Kang, B.; Ko, H.; Lee, J.; Shin, J.; Cho, K. Synthetic Tailoring of Solid-State Order in Diketopyrrolopyrrole-Based Copolymers Via Intramolecular Noncovalent Interactions. *Chem. Mater.* **2015**, *27*, 829−838.

(37) Zhang, X. R.; Richter, L. J.; DeLongchamp, D. M.; Kline, R. J.; Hammond, M. R.; McCulloch, I.; Heeney, M.; Ashraf, R. S.; Smith, J. N.; Anthopoulos, T. D.; Schroeder, B.; Geerts, Y. H.; Fischer, D. A.; Toney, M. F. Molecular Packing of High-Mobility Diketo Pyrrolo-Pyrrole Polymer Semiconductors with Branched Alkyl Side Chains. *J. Am. Chem. Soc.* **2011**, *133*, 15073−15084.

DOI: 10.1021/acsami.6b11737
ACS Appl. Mater. Interfaces 2017, 9, 9871−9879

(38) Meredig, B.; Salleo, A.; Gee, R. Ordering of Poly(3-Hexylthiophene) Nanocrystallites on the Basis of Substrate Surface Energy. *ACS Nano* **2009**, *3*, 2881−2886.
(39) Liu, F.; Wang, C.; Baral, J. K.; Zhang, L.; Watkins, J. J.; Briseno, A. L.; Russell, T. P. Relating Chemical Structure to Device Performance Via Morphology Control in Diketopyrrolopyrrole-Based Low Band Gap Polymers. *J. Am. Chem. Soc.* **2013**, *135*, 19248−19259.
(40) Chua, L. L.; Zaumseil, J.; Chang, J. F.; Ou, E. C. W.; Ho, P. K. H.; Sirringhaus, H.; Friend, R. H. General Observation of N-Type Field-Effect Behaviour in Organic Semiconductors. *Nature* **2005**, *434*, 194−199.
(41) Lee, W. H.; Park, J.; Kim, Y.; Kim, K. S.; Hong, B. H.; Cho, K. Control of Graphene Field-Effect Transistors by Interfacial Hydrophobic Self-Assembled Monolayers. *Adv. Mater.* **2011**, *23*, 3460−3464.
(42) Kang, B.; Kim, R.; Lee, S. B.; Kwon, S. K.; Kim, Y. H.; Cho, K. Side-Chain-Induced Rigid Backbone Organization of Polymer Semiconductors through Semifluoroalkyl Side Chains. *J. Am. Chem. Soc.* **2016**, *138*, 3679−3686.
(43) Rolland, A.; Richard, J.; Kleider, J. P.; Mencaraglia, D. Electrical Properties of Amorphous Silicon Transistors and Mis-Devices: Comparative Study of Top Nitride and Bottom Nitride Configurations. *J. Electrochem. Soc.* **1993**, *140*, 3679−3683.
(44) Zhang, W. M.; Han, Y.; Zhu, X. X.; Fei, Z. P.; Feng, Y.; Treat, N. D.; Faber, H.; Stingelin, N.; McCulloch, I.; Anthopoulos, T. D.; Heeney, M. A Novel Alkylated Indacenodithieno[3,2-B]Thiophene-Based Polymer for High-Performance Field-Effect Transistors. *Adv. Mater.* **2016**, *28*, 3922−3927.
(45) Kalb, W. L.; Batlogg, B. Calculating the Trap Density of States in Organic Field-Effect Transistors from Experiment: A Comparison of Different Methods. *Phys. Rev. B: Condens. Matter Mater. Phys.* **2010**, *81*, 035327−035339.
(46) Chen, M. S.; Niskala, J. R.; Unruh, D. A.; Chu, C. K.; Lee, O. P.; Frechet, J. M. J. Control of Polymer-Packing Orientation in Thin Films through Synthetic Tailoring of Backbone Coplanarity. *Chem. Mater.* **2013**, *25*, 4088−4096.
(47) Podzorov, V.; Menard, E.; Borissov, A.; Kiryukhin, V.; Rogers, J. A.; Gershenson, M. E. Intrinsic Charge Transport on the Surface of Organic Semiconductors. *Phys. Rev. Lett.* **2004**, *93*, 086602−086605.
(48) Sirringhaus, H. Device Physics of Solution-Processed Organic Field-Effect Transistors. *Adv. Mater.* **2005**, *17*, 2411−2425.

DOI: 10.1021/acsami.6b11737
ACS Appl. Mater. Interfaces 2017, 9, 9871−9879